# Fluid–Structure Interaction Model of a Percutaneous Aortic Valve: Comparison with an In Vitro Test and Feasibility Study in a Patient-Specific Case

Accepted manuscript at https://doi.org/10.1007/s10439-015-1429-x

# FLUID-STRUCTURE INTERACTION MODEL OF A PERCUTANEOUS AORTIC VALVE: COMPARISON WITH AN IN VITRO TEST AND FEASIBILITY STUDY IN A PATIENT-SPECIFIC CASE

Wei Wu[1], Desiree Pott[2], Beniamino Mazza[1], Tommaso Sironi[1], Elena Dordoni[1], Claudio Chiastra[1,3], Lorenza Petrini[4], Giancarlo Pennati[1], Gabriele Dubini[1], Ulrich Steinseifer[2], Simon Sonntag[2], Maximilian Kuetting[2], Francesco Migliavacca[1]

[1] Laboratory of Biological Structure Mechanics, Chemistry, Materials and Chemical Engineering 'Giulio Natta' Department, Politecnico di Milano, Milan, Italy

[2] Department of Cardiovascular Engineering, Institute of Applied Medical Engineering, RWTH Aachen University and University Hospital Aachen, Aachen, Germany

[3] Department of Biomedical Engineering, Thoraxcenter, Erasmus University Medical Center, Rotterdam, The Netherlands

[4] Department of Civil and Environmental Engineering, Politecnico di Milano, Milan, Italy

Address for correspondence:

Francesco Migliavacca, PhD

Laboratory of Biological Structure Mechanics, Chemistry, Materials and Chemical Engineering 'Giulio Natta' Department,

Politecnico di Milano,

Piazza Leonardo da Vinci, 32

20133 Milan - Italy

Phone: +39.02.2344.4316

E-mail: francesco.migliavacca@polimi.it

Accepted manuscript at https://doi.org/10.1007/s10439-015-1429-x

**Abstract** —— Transcatheter aortic valve replacement (TAVR) represents an established recent technology in a high risk patient base. To better understand TAVR performance, a fluid-structure interaction (FSI) model of a self-expandable transcatheter aortic valve was proposed. After an in vitro durability experiment was done to test the valve, the FSI model was built to reproduce the experimental test. Lastly, the FSI model was used to simulate the virtual implant and performance in a patient-specific case. Results showed that the leaflet opening area during the cycle was similar to that of the in vitro test and the difference of the maximum leaflet opening between the two methodologies was of 0.42 %. Furthermore, the FSI simulation quantified the pressure and velocity fields. The computed strain amplitudes in the stent frame showed that this distribution in the patient-specific case is highly affected by the aortic root anatomy, suggesting that the in vitro tests that follow standards might not be representative of the real behavior of the percutaneous valve. The patient-specific case also compared in vivo literature data on fast opening and closing characteristics of the aortic valve during systolic ejection. FSI simulations represent useful tools in determining design errors or optimization potentials before the fabrication of aortic valve prototypes and the performance of tests.

**Keywords** ~~fluid~~-structure interaction, valve mechanics, mathematical models, stent, transcatheter aortic valve.

## Introduction

Transcatheter aortic valve replacement (TAVR), firstly introduced in 2002 by Cribier[11], is a minimally-invasive procedure which is being adopted more and more in the treatment of valvular diseases. The procedure is performed by inserting a stented valve in the aortic root by means of a catheter. This technique is often used for people with symptomatic aortic stenosis for a standard valve replacement surgery. While TAVR represents an established technology in a high risk patient base and has delivered results which show that it is a match for surgical therapy in select groups of patients, many influential factors determining prosthesis performance are still not well understood. In this regard it should be considered that even though it is now 15 years after Bonhoeffer's first implantation of a balloon expandable valve with a platinum-iridium stent frame in the pulmonary position[4], and 13 years have passed since the first aortic valve implantation of a balloon expandable valve by Cribier in 2002[11], the first Nitinol based transcatheter valve was only implanted in 2006[16]. Additionally, the first Nitinol stent frames used non-complex geometries, based largely on experience gained with vascular stents. Much of the commonly cited experience with transcatheter valves is based on balloon expandable valves[38] or early Nitinol valves[40], while current developments focus more and more on complex Nitinol stent frames for the aortic and mitral position. The experience gained with plastically deformed balloon expandable devices cannot directly be transferred to Nitinol.

The trend to lower crimping diameters and more complex anatomically adapted geometries frequently tests the limits of stent frame durability during the in vitro testing phase. Unexpected stent frame fractures lead to high development costs and can potentially suffocate promising concepts. Like in other cardiovascular fields, *in silico* models have been applied to better understand the mechanics and hemodymanics of devices and treated vessels; in the aortic root pathologies they are emerging as useful tools for the prediction and the interpretation of the phenomena involved

and for the design optimization to increase durability and reduce several risk factors such as obstruction of coronary arteries, valve regurgitation[34] and hemolysis[19].

The behavior of a percutaneous valve is influenced either by the mechanics of the aortic root, the leaflets and the stent frame as well as the fluid passing through the site where the valve is implanted. Experimental studies for the investigation of TAVR have a low spatial resolution[2, 35] and many flow and structural characteristics either cannot be evaluated, or can only be evaluated with difficulty. In the literature, mathematical models related to TAVR are increasing. They can be related to the understanding of the mechanical behavior of the stented valve, the aortic root and the leaflet dynamics from a structural point of view[3, 6, 14, 17, 23, 32, 39] or to the hemodynamics inside the treated aortic root[3, 13, 31, 37]. To the best of our knowledge, scientific publications which take into account both the mechanical and the fluid aspects in a coupled manner are absent. Fluid-structure interaction (FSI) is emerging as a powerful tool for the study of biomechanical problems[33], and has been successfully applied for example to study the aortic root behavior in the presence of native valves[1, 7, 8, 12, 15, 18, 22, 24, 29, 36, 41-43].

In this context, the present paper aims to develop an FSI model for the study and evaluation of percutaneous aortic valves. In particular, *i*) we used an in vitro durability tester to test a realistic stented aortic valve, *ii*) we reproduced the in vitro conditions with an FSI simulation and *iii*) compared the results to verify the goodness of the numerical model. Successively, *iv*) we showed how FSI models are feasible to be used in patient-specific cases, which allowed reliable and more exhaustive information on the valve behavior to be obtained.

## Materials and methods

*The valve.* The valve used in this study (Fig. 1a) was purposely designed according to criteria common to stented aortic valves. The stent frame was laser-cut from a Nitinol tube, expanded to its

designated shape under heat treatment and then electropolished. Valve leaflets were made of polyurethane with a constant thickness of 0.16 mm. The leaflets were made from a cylindrical thin foil and glued from the outside to the stent frame. Finally, the valve was inserted in a silicone compartment representing the aortic root (Fig. 1.b).

*In vitro tests.* The valve sample was tested inside the CVE FT-2 accelerated durability tester (Fig. 2) at 600 bpm (beats per minute). The tester was filled with distilled water at 37° C as usually adopted in durability tests. A wobble plate generates a sinusoidal flow through the valves by compression and expansion of a bellows mounted under the mounting plate, on which the bottoms of test compartments are fixed. With compression of the bellows, the leaflets open. With expansion, a negative pressure is generated; the leaflets close and the fluid flows from above the valve to below the valve via an adjustable bypass. Pressures are measured directly upstream and downstream the valve. The stroke and the bypasses of the compartments were adapted (and held constant throughout the test) to obtain a good performance of the valve with proper opening and closing of the leaflets, while adjusting the pressure curve according to ISO 5840:3 (5% of the cycle over 100 mmHg pressure gradient over the valve). In total, the valves reached 10^7 cycles. A high speed video system mounted on top of the test compartments was used to record the motion of the leaflets.

*FSI model for in vitro case*

All the simulations were carried out with the explicit finite element commercial solver ANSYS LS-DYNA 971 release 7.0 (LSTC, Livermore CA, USA and ANSYS, Inc., Canonsburg, PA, USA) on an Intel Xeon workstation of 2.40 GHz with 8 processors. The solver not only has the well-known advantages on complicated contact behaviors, but also can handle FSI simulation using an arbitrary Lagrangian-Eulerian (ALE) technique. The three-dimensional geometrical models were created by Rhinoceros

5.0 (Robert McNeel & Associates, USA) and the meshing procedure was done by ICEM 15.0 (ANSYS, Inc., Canonsburg, PA, USA.).

The stent, leaflets and compartment were modeled using the dimensions of the final valve prototype (Figs. 1a and b) measured directly on the samples. The leaflet model was connected with the valve model using a tied-type contact method to mimic the glue between stent and leaflets. A self-contact among the top three leaflets was set up throughout valve deployment and fatigue cycles. Twelve rigid planes (not shown here) uniformly around the valve model crimped the valve model to the outer diameter less than the inner diameter of the compartment model, then released the valve model into the compartment model (Fig. 1b). A tied-type contact was activated between the valve and compartment model when the valve was released, which means once the valve model was implanted, the sliding between the model interfaces was prohibited. The detailed definition of these contacts is listed in Table 1.

The stent frame was modeled with 28,296 8-node hexahedral elements with reduced integration points. The mechanical properties of superelastic NiTi were obtained from tensile tests on original tubes for the valve stent. First, wire specimens were cut from the NiTi tubes, electro-polished and heat-treated to get the similar properties of the valve stent, as done by Petrini et al.[26]. Then, static tensile tests were carried out using an MTS 858 Mini Bionix servo-hydraulic testing machine according to the methodology prescribed in the standard ASTM F 2516-07 in temperature controlled conditions (37°C): tension loading up to 6% of strain, unloading up to initial configuration and again tension loading up to fracture. The mechanical parameters of the NiTi used in the simulations are reported in Table 2. The density of NiTi was set to 6,450 kg/m$^3$.

For the valve leaflets, the model was discretized by 4,938 4-node full-integration shell elements. They were modeled as an elastic material with a Young modulus of 8 MPa, a Poisson's ratio of 0.49

and a density of 2,600 kg/m$^3$. The assumption of an elastic material makes the simulation much more stable than that with more sophisticated material models, especially when complex contact behaviors of the leaflets are taken into account. The silicon compartment model was discretized with 18,465 8-node hexahedral full-integration elements. Its Young modulus was set to 2.2 MPa, Poisson's ratio to 0.49 and density to 2,600 kg/m$^3$.

The FSI model was composed of structural parts coupled with fluid parts using an immersed boundary method (Fig. 1c): In brief, the outer surface of the solid parts will "cut" the unconformable fluid elements that it overlaps, and the resulting fluid elements inside the solid domain will be handled as a "void" domain. During the simulation, the code searches for the penetration of the solid surface into the fluid domain (excluding the "void" domain), and elastic action-reaction forces are generated to push the penetrating structural elements back from fluid parts by means of a penalty-based coupling approach, through which the structural-fluid interaction is created. More details about this method can be found in references[15, 28].

The fluid parts consist of a control volume (fluid domain), inlet and outlet parts. Since in the in vitro experiment the bottom of the compartment is fixed and fluid has no influence on the bottom during testing cycles, only the structural parts over the compartment bottom were immersed in the fluid domain. Two penalty couplings were set to handle the interactions between the fluid and the leaflets, and between the fluid and the compartment. The interaction between the fluid and the stent was not considered for two reasons: first, the movement of the stent during fatigue testing is mostly controlled by the compartment and the leaflets, and the influence of the stent on fluid dynamics can be neglected compared to that of the compartment and the leaflets; second, the stent was meshed with elements of much smaller size than those of fluid domain elements because of the valve's "slim" dimension. If the fluid domain was meshed with elements compatible to those of the stent, the whole model would have an exorbitant simulation cost.

The discretization of the fluid parts resulted in a number of element equal to 68,837 after a proper grid sensitivity analysis. The utilized elements were 8-node hexahedral Eulerian elements with single integration points. The fluid (water) was assumed Newtonian with a density of 1000 kg/m$^3$ and a dynamic viscosity of 7e-4 Pa·s (at 37° C). To reduce the simulation time, a bulk modulus of 22 MPa was used as proposed by Lau et al[20].

As a boundary condition for the structural part, only the bottom of the compartment model was fixed in all directions. For the fluid part, the pressure curve measured upstream in the *in vitro* test was applied to the inlet section (Fig. 3), representing the transvalvular gradient with a peak value of 108 mmHg. For the outlet section, a zero pressure was applied. All the nodes at the outer surfaces of the fluid part were fixed in all directions.

The FSI simulation was carried out in the following steps: first, the valve was crimped and implanted into the compartment, which took 0.4 s. In this step the two FSI couplings were deactivated and the pressure of the inlet and outlet was kept at zero. After that, the two FSI couplings were activated and the pressure of the inlet began to follow the pressure gradient of the in vitro test. Three cycles (0.1 s each according to 600 bpm of in vitro test) were undertaken to ensure a stable response of the simulation (Fig.3).

One critical point of the simulation is the timestep selection. Since the size of the stent element is very tiny, the smallest stable timestep is about 8e-9 s, which requires more than one month to finish the FSI simulation for the in vitro case based on current computation resources; thus, a mass scaling strategy was chosen to decrease the simulation time. However, this strategy may introduce unwanted inertial effects that adversely affect the results. Hence, a timestep was chosen with which only the stent model was mass-scaled. The kinetic energy of the stent model with this timestep was intensely monitored throughout the simulation to guarantee that the fraction of its kinetic and

internal energy was always less than 5%, which means that the artificially introduced inertial effect is acceptable.

As for the results, the time period from 0.575 s to 0.675 s was chosen to illustrate a "closed-open-closed" leaflet cycle (Fig. 3). In this period of 0.1 s, five time points were set to get the applicable results: 0, 0.02, 0.035, 0.06, and 0.08 s.

*FSI model for the patient-specific case*

As a last part of this work, a patient-specific aortic root (AR) was obtained from a patient suffering from aortic stenosis. The 3D anatomy of stereo lithography (STL) format was reconstructed from CT images by means of Materialise software (Mimics and 3-matic, Materialise NV, Leuven, Belgium) (Fig. 4a). To segment the AR, a Hounsfield unit threshold mask was applied, followed by automated standard image processing tools (static and dynamic region growing) as well as morphologic operations and manual editing. Surface smoothing and wrapping processes were subsequently applied to fix inconsistencies in the model due to image noise. Then the STL file was trimmed at ventricular, aortic and coronary positions to get plane ends (Fig. 4a).

The fluid parts of the FSI model for the patient-specific case were created based on the configuration of the AR (Fig. 4b). The AR was totally immersed in the blood domain. Two penalty coupling of FSI simulation were set to handle the interactions between blood and leaflets, and between blood and AR. Inlet and outlet parts were set up at ventricular and aortic ends, respectively. Coronary vessels were not taken into account. An external boundary layer was used to provide a null extramural pressure. The deployment procedure of the valve into the AR is similar to that of the in vitro case and is shown in Fig. 4c. The same tied-type contact was set up between the stent and the AR model.

The AR model was discretized by 21,922 8-node hexahedral full-integration elements. The AR was assumed to have an elastic behavior with a Young modulus of 2 MPa, a Poisson's ratio of 0.3 and a

density of 1,100 kg/m$^3$ [36]. The total number of 8-node hexahedral Eulerian elements with a single integration point for the fluid parts was 108,580. Blood was assumed a Newtonian fluid with a dynamic viscosity of 0.0035 Pa·s and a density of 1,060 kg/m$^3$.

As boundary conditions, the AR model was fixed at ventricular, aortic and coronary ends in all directions. For the fluid part, ventricular and aortic pressure tracings (Fig. 5) were applied at the inlet and outlet sections of the AR model, respectively. For the sake of comparison with the previous experimental test, the peak transvalvular gradient also reached 108 mmHg. All the nodes at the outer surfaces of the fluid part were fixed in all directions.

The simulation was carried out in the following steps (Fig. 5): first, the valve was crimped and implanted into the AR, which took 0.4 s. In this step the two couplings of FSI were deactivated, but the pressure of all the fluid parts was increased to 80 mmHg as pressure initialization. Afterwards, the two FSI couplings were activated and the pressure of the inlet and outlet began to follow their pressure tracing respectively. The pressure of the external boundary layer was decreased to zero in a short time (0.1 s) to provide a null extramural pressure out of the vessel. Finally, three cycles (0.8 s each) were undertaken and a similar timestep as in the in vitro case was used; the artificially introduced inertial effect of the stent model was guaranteed to be acceptable.

As for the results, the five time points chosen to illustrate them were: 0, 0.02, 0.04, 0.4, and 0.64 s from the beginning of each cardiac cycle.

The FSI simulations can provide plenty of results for both fluid and structural parts. The following will be shown for the in vitro and patient-specific cases: leaflet kinematics, velocity and pressures fields, stress and strain changes of the stent, and the compliance of compartment ($C_{com}$) and aorta ($C_{aor}$) during test and cardiac cycles. In particular, the alternating ($\varepsilon_a$) and mean ($\varepsilon_m$) first principal strains during one cycle will be evaluated to see the difference on stent fatigue behavior of the two

cases: $\varepsilon_a = (\varepsilon_{max} - \varepsilon_{min})/2$, and $\varepsilon_m = (\varepsilon_{max} + \varepsilon_{min})/2$ where $\varepsilon_{max}$ and $\varepsilon_{min}$ are the maximum and minimum first principal strain during one cycle, respectively. Compliances are evaluated as: $C = (D_{sys} - D_{dia})/D_{avg} \times 100\%$ where the $D_{sys}$ and $D_{dia}$ are the compartment or AR diameter at the "commissure" locations of the leaflets at systole and diastole during one cycle, respectively; and $D_{avg}$ is the averaged diameter. 15 and 150 hours were necessary to carry out the in vitro and patient-specific FSI simulations, respectively.

## Results

### *In vitro tests*

The experiment allowed visualization of the valve kinematics during the cycle. Results of the leaflets' kinematics are reported in terms of leaflet open area during the tested cycle (Figs. 6 and 7).

### *FSI model for the in vitro case*

A direct comparison of the leaflets opening in five instances is reported (Fig. 6) to compare the results from the FSI simulation and experiment. The leaflet open area curve plotted as function of the tested cycle time calculated from FSI simulations is superimposed onto the experimental one in Fig. 7. The difference between in vitro and in silico results at the maximum opening area is 0.42%. Furthermore, from the simulations the pressure and velocity fields during the valve opening and closing can be displayed (Fig. 8a and b). Pathlines with respect to velocities are also displayed (Fig. 8c). The compliance of the compartment $C_{com}$ was evaluated as 12.3 %.

In addition, a simulation like the one performed allows researchers to analyze the stress and strain distribution inside the stent, the leaflets and the compartment. Fig. 9a depicts the distribution of an alternating first principal strain in the stent frame. The areas with the highest values are envisaged. One stent element (number of 56551) was chosen to show its stress-strain changes during the whole simulation (Fig. 9b).

*FSI model for the patient-specific case*

The leaflets movement, deformation of valve and aorta during the whole cardiac cycle are shown in regards to leaflet kinetics (Fig. 10a). Furthermore, since the leaflet kinetics during the systolic ejection have been studied in vivo semi-quantitatively[21], a comparison was made between the in vivo measured results and FSI simulation focused on the period of systolic ejection (Fig. 11). Three nodes at the middle of the upper leaflet edges were chosen to calculate their radius displacements during the ejection time. For illustration convenience, the original position of each node was set when the radial displacement began to increase (0.015 s). According to the reference, the rapid valve opening (RVOT) and closing (RVCT) time can be calculated when the radial displacement curves of the nodes have severe increases and decreases, respectively. Ten time points were also selected to provide the detailed reference of rapid leaflet opening and closing. The calculated RVOT, RVCT and ejection time (ET) were listed in Table 3 and compared to fast opening and closing leaflet characteristics of in vivo measurements[21].

Figs. 10b-c show the results in terms of pressure and velocity contour maps as well as pathlines in the patient-specific model over the cardiac cycle. The compliance of the aorta $C_{aor}$ was evaluated as 8.03%.

Figure 12 reports the alternating strain distribution map in the stent frame with the locations having the highest values. The fatigue life diagrams, in terms of alternating and mean strains for the stented valve when tested in the silicone compartment and when inserted in the patient-specific AR, are superimposed in the same figure. A direct comparison with a widely accepted literature fatigue curve[25] is provided. It can be noted that in the patient specific case, there are a few elements that are more subjected to fatigue fracture, and in general, the distribution of the strain is very different between the in vitro and the patient-specific cases.

## Discussion

The present study reports an insight into aortic transcatheter valves by means of verified numerical simulations with the aim to demonstrate the feasibility of the evaluation of TAVR prostheses. Although in recent years numerical studies in this field have emerged, as far as the authors are aware, fluid-structure simulations of percutaneous valves are absent. Only structural[3, 6, 14, 17, 23, 32, 39] or fluid dynamics[3, 13, 31, 37] studies have been carried out. This study used fluid-structure interaction simulations both in the in vitro durability testing and in the patient-specific set-up. The experimental testing was based on ISO 5840:3 and FDA guidance draft standards to evaluate the performance of a purposely designed shape memory alloy transcatheter valve. The comparison in terms of leaflet opening area between the in vitro test and the simulation produced small differences at the maximum opening and allow us to have an acceptable verification of the goodness of the simulation itself. In some time instances, the differences between the in vitro and in silico tests were more pronounced, but important parameters, like the beginning of valve opening, beginning of valve closing and moment of maximum valve opening, were similar. Furthermore, a deeper process of validation would be required with measurements of other quantities like velocities (for example by means of particle image velocimetry) or stent frame deformation. However, these initial results support our findings and the correctness of the numerical methodology we used to give insights into the behavior of these devices that measure quantities not easily accessible in an experiment or in an in vivo setup. Indeed, velocity and pressure fields, viscous shear stress, areas of abnormal hemodynamics with recirculations, vortices, leakages, stresses and strains in the valve, in the leaflets, in the vascular tissues and struts malposition are useful indications to estimate whether a valve implant is performed with the highest probability of success. Fluid-structure simulations have the great advantage to combine both structural aspects and hemodynamics. This is very important in order to predict, for example, the leaflet kinematics which influences the hydrodynamic

performance, durability and hemocompatibility of the prostheses. A stand-alone structural simulation requires particular boundary conditions that in turn can be affected by the fluid dynamics generated by the presence of the valve. These constraints cannot be easily estimated in real life and usually are imposed as 'reasonable' boundaries in the simulations. Conversely, a stand-alone fluid dynamic simulation neglects the movement and the presence of the surrounding tissues, like the valve annulus and, the aortic root, which influence the movements and the dynamics of the valve.

One of the main results from this study is that numerical FSI simulations carried out on patient-specific cases can be used to predict the behavior of the valve and support clinical decisions[5]. Indeed, this study showed some differences in the valve behavior between the in vitro and in vivo situations. A uniformly deployed configuration, which is the conventional method employed in bench testing protocols, might predict a stress state completely different with respect to the in vivo situation. By especially considering the intended lower crimping diameters and more complex anatomically adapted geometries of prostheses currently under development, questions are raised on durability testing approaches and regulatory requirements. Hence, simulations like those here proposed can, on one side, be used to re-design, refine and propose new standards for the preclinical evaluation of medical devices, and on the other side, study individual cases for a better prediction of the device behavior. Additionally, the comparison of the fluid dynamics fields of the in vitro and in vivo cases (Figs. 8 and 10) allow researchers to visualize the differences in streamlining, vortices and hemodynamic complexity. For example, the maximum velocities were higher in the in vivo test, although the pressure gradient applied was similar but with a different cycle duration. The quantification of these differences along with the clinical outcome of these procedures might allow us to refine the in vitro tests with loading conditions representative of the worst clinical scenario and, thus, allow for an evaluation of the valve performance under more realistic conditions. From the in vivo simulation, other important parameters, like shear stresses, can be evaluated. This will

allow us to identify, for example, the most important risk factors of hemolysis after a TAVI procedure. The recent study by Laflamme and colleagues (REF) identify wall shear rate[9] and the energy loss index[27] as risk factors in patient with severe prosthesis-patient mismatch. Numerical simulations have the theoretical advantage over experimental studies for the investigation of TAVR to overcome the limit of the spatial resolution[2, 35], which makes the evaluation of many in vivo flow and structural characteristics very difficult.

The patient-specific model studied here also has the advantage that the interaction between a transcatheter valve and the implantation site can be assessed. In vitro durability test methods for transcatheter valves are largely based on those for surgical bioprostheses. While these maintain their shape after implantation, transcatheter valves interact with the anatomy and are frequently non-round following implantation[10]. This potentially influences the durability of the device[30]. Studying this effect has only been possible in a clinical setting thus far.

The simulations carried out in this work are not absent of limitations. Regarding the fluid part, turbulence was neglected. For the patient-specific case, the pressure curves used as boundary conditions were not those of the patient. Also, the coronary arteries and the native valve leaflets were not considered. These facts make the simulation not representative of the real situation and any obstruction generated by the valve position on the coronary perfusion is not considered. The hemodynamics patterns found in this work are different from the specific ones in the in vivo situation, but are still representative of a realistic situation. Clearly, the objective of this work was not the detailed description of the fluid dynamics of a particular patient, but to evaluate if virtual implantation and FSI simulation in a specific patient are feasible. The inclusion of the coronary circulation is a future step to have a more realistic and predictive model, e.g. to investigate coronary obstruction in detail. For the structural part, the aortic root was modeled as a linear elastic material without any calcified area. A better description of the real behavior of the aortic root, now possible

with imaging techniques, as the computed tomography, might influence the deployment of the valve. Calcified areas may lead to areas where the stent frame is malpositioned with great influence on potential regurgitant flows. Valve leaflets were considered elastic; experimetal tests on this material were carried out to verify the correctness of this assumption. Additionally, the fatigue life diagram of Fig. 12 is taken from literature. For a correct estimation of the real behavior of the valve in terms of fatigue failure, the real fatigue life diagram should be built from ad hoc experimental tests, as each NiTi material has its own curve. The purpose of this paper was not the study of the fatigue behavior of this realistic valve but to show how numerical simulations can replicate in vitro tests by adding some information that is not easily available from experimentations. Further studies will explore the fatigue behavior of percutaneous valves with FSI simulations.

The use of advanced, verified, in silico models during the early development stages of a novel transcatheter valve have the potential to expedite the development process and, save time and money. The developed methods represent useful tools in determining design errors or optimization potentials before the fabrication of prototypes and the performance of tests. They thereby help advance the technology of TAVR and make it safer, which will be crucial should this therapy transition to lower risk patients.

## Conflict of interests

There is no conflict of interests.

## Acknowledgements

Wei Wu is supported by the Politecnico di Milano International Fellowships Program (PIF). Claudio Chiastra is partially supported by the ERC starting grant (310457, BioCCora). Desiree Pott is supported by the Deutsche Forschungsgemeinschaft (DFG) grant STE1680/5-1.

## References

[1]Astorino M., J.-F. Gerbeau, O. Pantz and K.-F. Traore. Fluid-structure interaction and multi-body contact: Application to aortic valves. *Comput. Methods. Appl. Mech. Eng.* 198: 3603-3612, 2009.

[2]Azadani A. N., N. Jaussaud, P. B. Matthews, L. Ge, T. S. Guy, T. A. M. Chuter and E. E. Tseng. Energy loss due to paravalvular leak with transcatheter aortic valve implantation. *Ann. Thorac. Surg.* 88: 1857-1863, 2009.

[3]Bianchi M., R. Ghosh, D. Das, G. Marom, T. Claiborne, M. Slepian and D. Bluenstein. Transcatheter aortic valve replacement model: crimping and deploying in patient-pathology specific roots. In: *Summer Biomechanics, Bioengineering and Biotransport Conference*. Snowbird Resort, Utah, USA: 2015.

[4]Bonhoeffer P., Y. Boudjemline, Z. Saliba, J. Merckx, Y. Aggoun, D. Bonnet, P. Acar, J. Le Bidois, D. Sidi and J. Kachaner. Percutaneous replacement of pulmonary valve in a right-ventricle to pulmonary-artery prosthetic conduit with valve dysfunction. *Lancet* 356: 1403-1405, 2000.

[5]Bosi G. M., C. Capelli, S. Khambadkone, A. M. Taylor and S. Schievano. Patient-specific finite element models to support clinical decisions: A lesson learnt from a case study of percutaneous pulmonary valve implantation. *Catheter. Cardiovasc. Interv.* DOI: 10.1002/ccd.25944, 2015.

[6]Capelli C., G. M. Bosi, E. Cerri, J. Nordmeyer, T. Odenwald, P. Bonhoeffer, F. Migliavacca, A. M. Taylor and S. Schievano. Patient-specific simulations of transcatheter aortic valve stent implantation. *Med. Biol. Eng. Comput.* 50: 183-192, 2012.

[7]Carmody C. J., G. Burriesci, I. C. Howard and E. A. Patterson. An approach to the simulation of fluid-structure interaction in the aortic valve. *J. Biomech.* 39: 158-169, 2006.

[8]Chandra S., N. M. Rajamannan and P. Sucosky. Computational assessment of bicuspid aortic valve wall-shear stress: implications for calcific aortic valve disease. *Biomech. Model. Mechanobiol.* 11: 1085-1096, 2012.

[9]Cho Y.-I. and D. J. Cho. Hemorheology and Microvascular Disorders. *Korean Circulation Journal* 41: 287-295, 2011.

[10]Cosentino D., M. A. Quail, G. Pennati, C. Capelli, P. Bonhoeffer, V. Diaz-Zuccarini, A. M. Taylor and S. Schievano. Geometrical and stress analysis of factors associated with stent fracture after melody percutaneous pulmonary valve implantation. *Circ. Cardiovasc. Interv.* 7: 510-517, 2014.

[11]Cribier A., H. Eltchaninoff, A. Bash, N. Borenstein, C. Tron, F. Bauer, G. Derumeaux, F. Anselme, F. Laborde and M. B. Leon. Percutaneous transcatheter implantation of an aortic valve prosthesis for calcific aortic stenosis - First human case description. *Circulation* 106: 3006-3008, 2002.

[12]De Hart J., F. P. T. Baaijens, G. W. M. Peters and P. J. G. Schreurs. A computational fluid-structure interaction analysis of a fiber-reinforced stentless aortic valve. *J. Biomech.* 36: 699-712, 2003.

[13]Dwyer H. A., P. B. Matthews, A. Azadani, N. Jaussaud, L. Ge, T. S. Guy and E. E. Tseng. Computational fluid dynamics simulation of transcatheter aortic valve degeneration. *Interact. Cardiovasc. Thorac. Surg.* 9: 301-308, 2009.

[14]Esterhuyse A., K. Van Der Westhuizen, A. Doubell, H. Weich, C. Scheffer and K. Dellimore. Application of the finite element method in the fatigue life prediction of a stent for a percutaneous heart valve. *J. Mech. Med. Biol.* 12: 2012.

[15]Griffith B. E. Immersed boundary model of aortic heart valve dynamics with physiological driving and loading conditions. *Int. J. Numer. Method. Biomed. Eng.* 28: 317-345, 2012.

[16]Grube E., J. C. Laborde, U. Gerckens, T. Felderhoff, B. Sauren, L. Buellesfeld, R. Mueller, M. Menichelli, T. Schmidt, B. Zickmann, S. Iversen and G. W. Stone. Percutaneous implantation of the CoreValve self-expanding valve prosthesis in high-risk patients with aortic valve disease - The Siegburg first-in-man study. *Circulation* 114: 1616-1624, 2006.

[17]Gunning P. S., T. J. Vaughan and L. M. McNamara. Simulation of self expanding transcatheter aortic valve in a realistic aortic root: implications of deployment geometry on leaflet deformation. *Ann. Biomed. Eng.* 42: 1989-2001, 2014.

[18]Hsu M.-C., D. Kamensky, Y. Bazilevs, M. S. Sacks and T. J. R. Hughes. Fluid-structure interaction analysis of bioprosthetic heart valves: significance of arterial wall deformation. *Comput. Mech.* 54: 1055-1071, 2014.

[19]Laflamme J., R. Puri, M. Urena, L. Laflamme, H. DeLarochelliere, O. A.-J. Altisent, M. del Trigo, F. Campelo-Parada, R. DeLarochelliere, J.-M. Paradis, E. Dumont, D. Doyle, S. Mohammadi, M. Cote, P. Pibarot, V. Laroche and J. Rodes-Cabau. Incidence and Risk Factors of Hemolysis After Transcatheter Aortic Valve Implantation With a Balloon-Expandable Valve. *Am. J. Cardiol.* 115: 1574-1579, 2015.

[20]Lau K. D., V. Diaz, P. Scambler and G. Burriesci. Mitral valve dynamics in structural and fluid-structure interaction models. *Med. Eng. Phys.* 32: 1057-1064, 2010.

[21]Leyh R. G., C. Schmidtke, H. H. Sievers and M. H. Yacoub. Opening and closing characteristics of the aortic valve after different types of valve-preserving surgery. *Circulation* 100: 2153-2160, 1999.

[22]Marom G., R. Haj-Ali, E. Raanani, H.-J. Schaefers and M. Rosenfeld. A fluid-structure interaction model of the aortic valve with coaptation and compliant aortic root. *Med. Biol. Eng. Comput.* 50: 173-182, 2012.

[23]Morganti S., M. Conti, M. Aiello, A. Valentini, A. Mazzola, A. Reali and F. Auricchio. Simulation of transcatheter aortic valve implantation through patient-specific finite element analysis: Two clinical cases. *J. Biomech.* 47: 2547-2555, 2014.

[24]Nobari S., R. Mongrain, E. Gaillard, R. Leask and R. Cartier. Therapeutic vascular compliance change may cause significant variation in coronary perfusion: A numerical study. *Comput. Math. Methods. Med.* 2012: 10 pages, 2012.

[25]Pelton A. R., V. Schroeder, M. R. Mitchell, X.-Y. Gong, M. Barney and S. W. Robertson. Fatigue and durability of Nitinol stents. *J. Mech. Behav. Biomed. Mater.* 1: 153-164, 2008.

[26]Petrini L., W. Wu, E. Dordoni, A. Meoli, F. Migliavacca and G. Pennati. Fatigue behavior characterization of nitinol for peripheral stents. *Funct. Mater. Lett.* 5: 2012.

[27]Pibarot P., D. Garcia and J. G. Dumesnil. Energy Loss Index in Aortic Stenosis From Fluid Mechanics Concept to Clinical Application. *Circulation* 127: 1101-1104, 2013.

[28]Puso M. A., J. Sanders, R. Settgast and B. Liu. An embedded mesh method in a multiple material ALE. *Comput. Methods. Appl. Mech. Eng.* 245: 273-289, 2012.

[29]Ranga A., O. Bouchot, R. Mongrain, P. Ugolini and R. Cartier. Computational simulations of the aortic valve validated by imaging data: evaluation of valve-sparing techniques. *Interact. Cardiovasc. Thorac. Surg.* 5: 373-378, 2006.

[30]Schievano S., A. M. Taylor, C. Capelli, P. Lurz, J. Nordmeyer, F. Migliavacca and P. Bonhoeffer. Patient specific finite element analysis results in more accurate prediction of stent fractures: Application to percutaneous pulmonary valve implantation. *J. Biomech.* 43: 687-693, 2010.

[31]Sirois E., Q. Wang and W. Sun. Fluid Simulation of a Transcatheter Aortic Valve Deployment into a Patient-Specific Aortic Root. *Cardiovasc. Engi. Tech.* 2: 186-195, 2011.

[32]Smuts A. N., D. C. Blaine, C. Scheffer, H. Weich, A. F. Doubell and K. H. Dellimore. Application of finite element analysis to the design of tissue leaflets for a percutaneous aortic valve. *J. Mech. Behav. Biomed. Mater.* 4: 85-98, 2011.

[33]Sonntag S. J., T. A. S. Kaufmann, M. R. Buesen, M. Laumen, T. Linde, T. Schmitz-Rode and U. Steinseifer. Simulation of a pulsatile total artificial heart: Development of a partitioned fluid structure interaction model. *J. Fluid. Struct.* 38: 187-204, 2013.

[34]Stahli B. E., W. Maier, R. Corti, T. F. Luscher, R. Jenni and F. C. Tanner. Aortic regurgitation after transcatheter aortic valve implantation: mechanisms and implications. *Cardiovasc. Diagn. Ther.* 3: 15-22, 2013.

[35]Stuehle S., D. Wendt, G. Hou, H. Wendt, M. Schlamann, M. Thielmann, H. Jakob and W. Kowalczyk. In-vitro investigation of the hemodynamics of the edwards sapien (TM) transcatheter heart valve. *J. Heart Valve Dis.* 20: 53-63, 2011.

[36]Sturla F., E. Votta, M. Stevanella, C. A. Conti and A. Redaelli. Impact of modeling fluid-structure interaction in the computational analysis of aortic root biomechanics. *Med. Eng. Phys.* 35: 1721-1730, 2013.

[37]Sun W., K. Li and E. Sirois. Simulated elliptical bioprosthetic valve deformation: Implications for asymmetric transcatheter valve deployment. *J. Biomech.* 43: 3085-3090, 2010.

[38]Toggweiler S., K. H. Humphries, M. Lee, R. K. Binder, R. R. Moss, M. Freeman, J. Ye, A. Cheung, D. A. Wood and J. G. Webb. 5-Year outcome after transcatheter aortic valve implantation. *J. Am. Coll. Cardiol.* 61: 413-419, 2013.

[39]Wang Q., S. Kodali, C. Primiano and W. Sun. Simulations of transcatheter aortic valve implantation: implications for aortic root rupture. *Biomech. Model. Mechanobiol.* 14: 29-38, 2015.

[40]Webb J. G. and D. A. Wood. Current status of transcatheter aortic valve replacement. *J. Am. Coll. Cardiol.* 60: 483-492, 2012.

[41]Weinberg E. J. and M. R. Kaazempur Mofrad. Transient, three-dimensional, multiscale simulations of the human aortic valve. *Cardiovasc. Eng.* 7: 140-155, 2007.

[42]Weinberg E. J., P. J. Mack, F. J. Schoen, G. Garcia-Cardena and M. R. K. Mofrad. Hemodynamic environments from opposing sides of human aortic valve leaflets evoke distinct endothelial phenotypes in vitro. *Cardiovasc. Eng.* 10: 5-11, 2010.

[43]Weinberg E. J. and M. R. K. Mofrad. A multiscale computational comparison of the bicuspid and tricuspid aortic valves in relation to calcific aortic stenosis. *J. Biomech.* 41: 3482-3487, 2008.

Accepted manuscript at https://doi.org/10.1007/s10439-015-1429-x

**Figures**

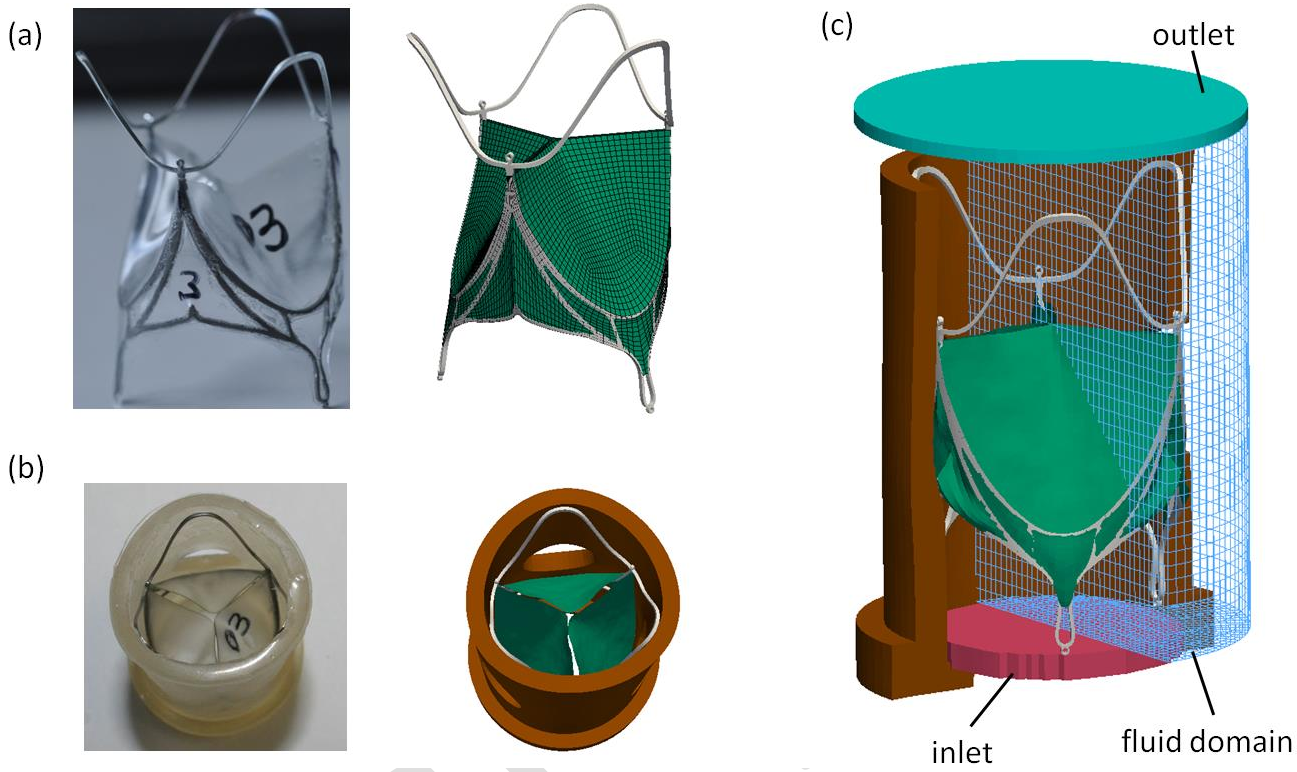


Figure 1. In vitro test setup and FSI models. (a) Stented valve and corresponding model where the leaflet mesh is visible. (b) The valve inserted in a silicon compartment representing the aortic root and the corresponding model. (c) FSI model including the valve, the compartment and the fluid domain; inlet and outlet sections are visible where the boundary conditions are applied in terms of pressures.

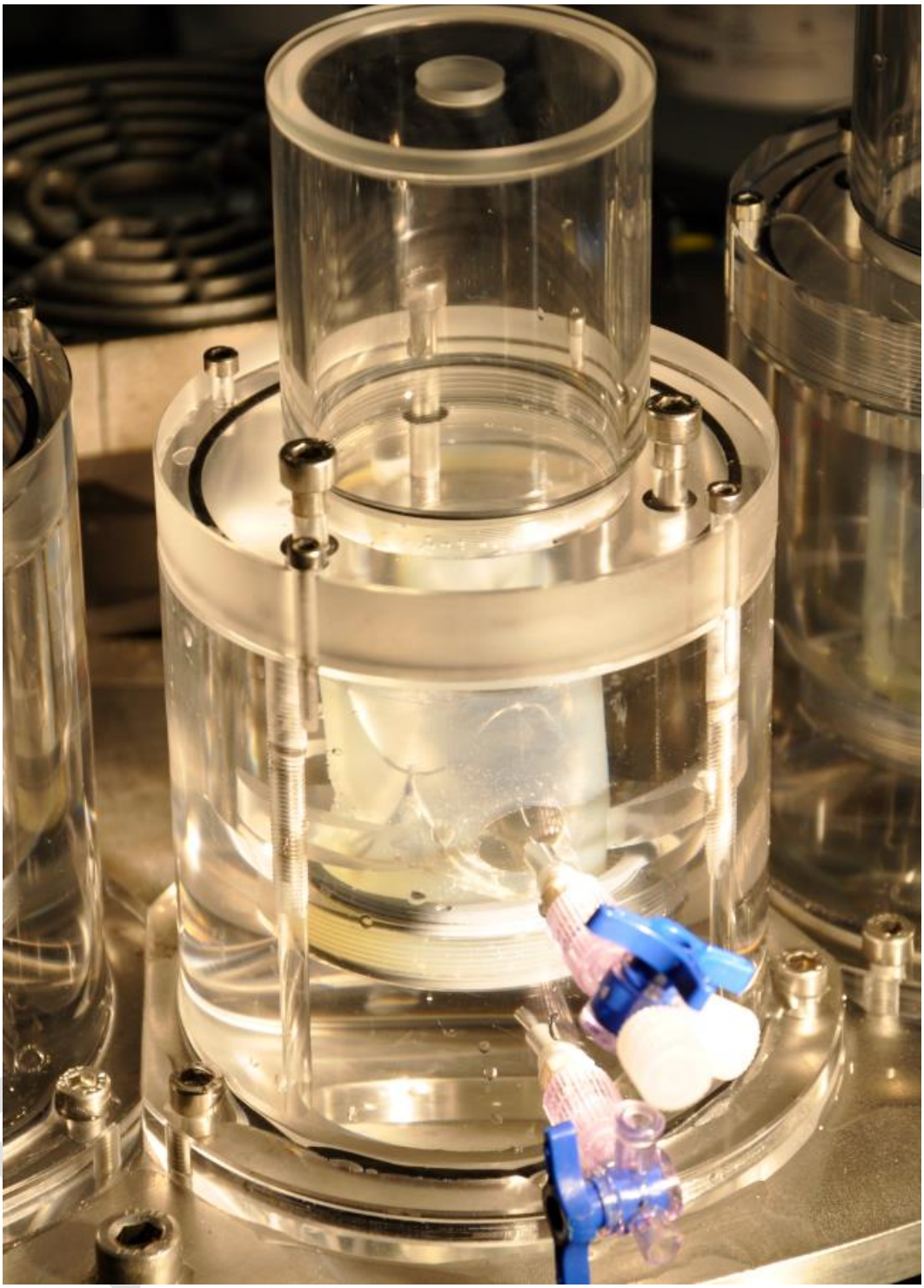

Figure 2. CVE FT-2 accelerated durability test system. The motion of the leaflets was recorded by a high speed video system mounted on top of the test compartments.

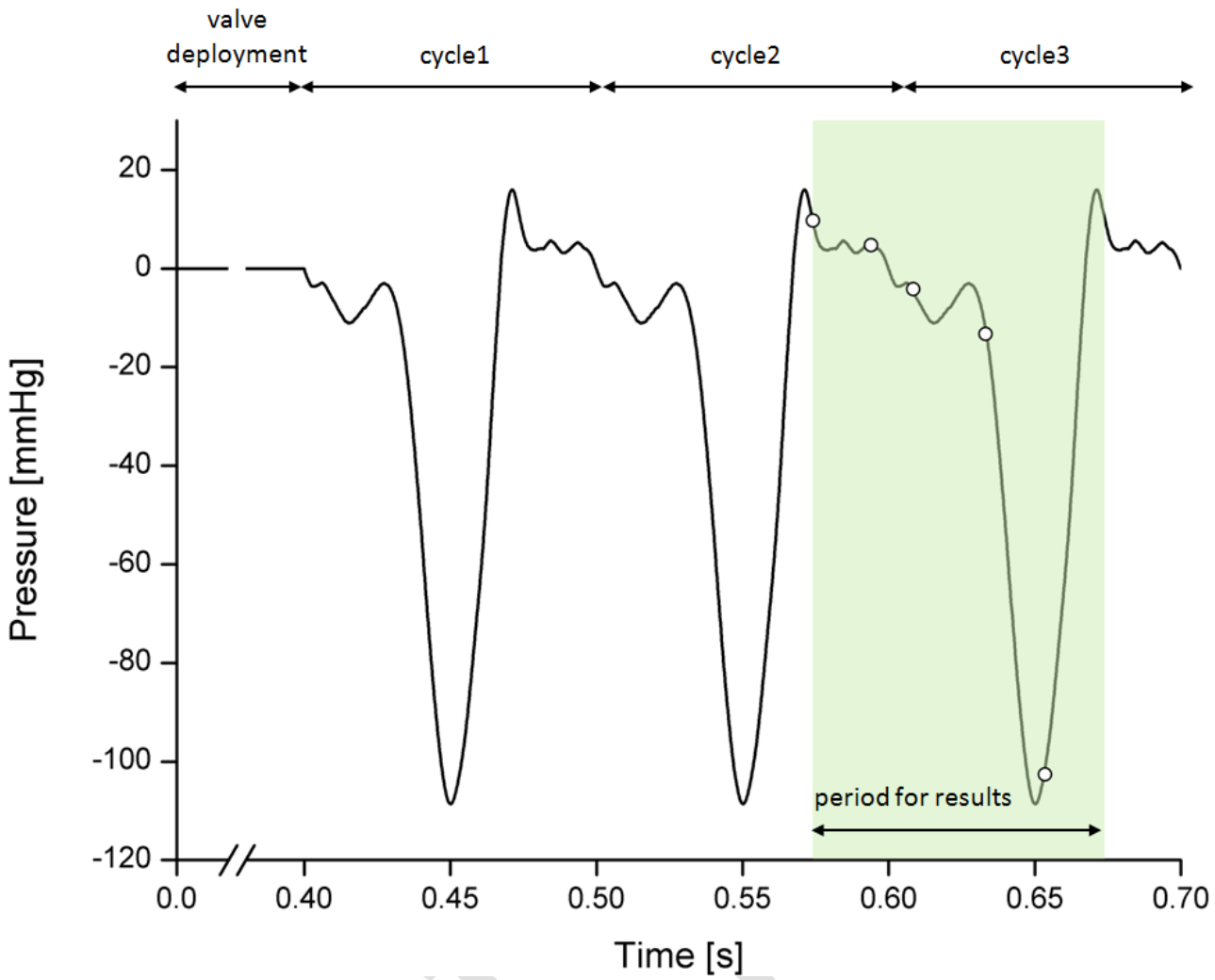


Figure 3. Pressure curve measured upstream from the valve during the in vitro test and imposed as a boundary condition in the FSI simulation at the inlet section. The first part of the tracing refers to the simulation of the valve deployment. Applicable results are from the second and third cycles (green area). Circles on the curve are the time points to show the results.

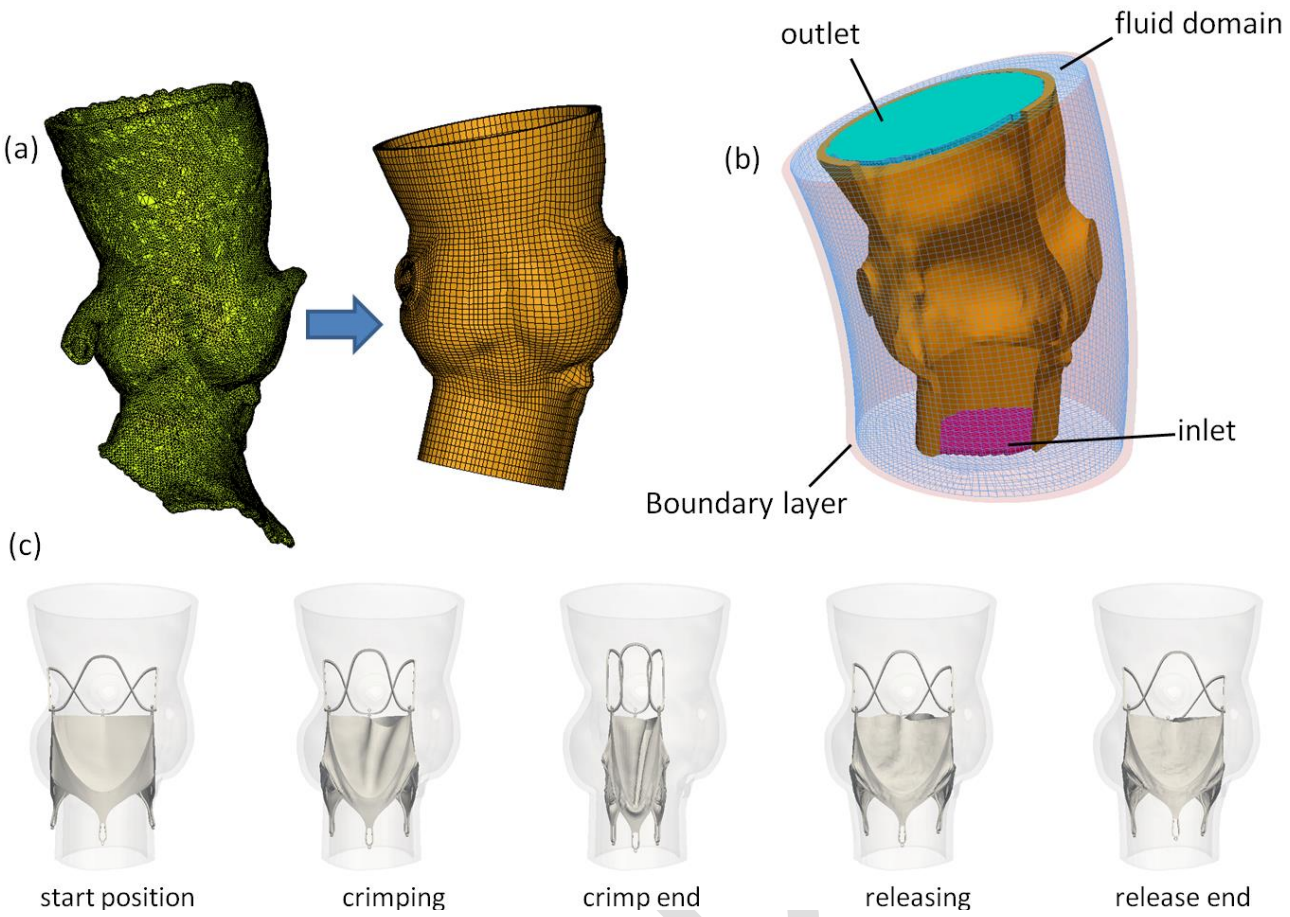


Figure 4. (a) Anatomy of the aortic root of the patient-specific case and meshes of the AR model; (b) FSI model with inlet, outlet, fluid domain and the boundary layer; c) the deployment procedure of the valve into the aortic root.

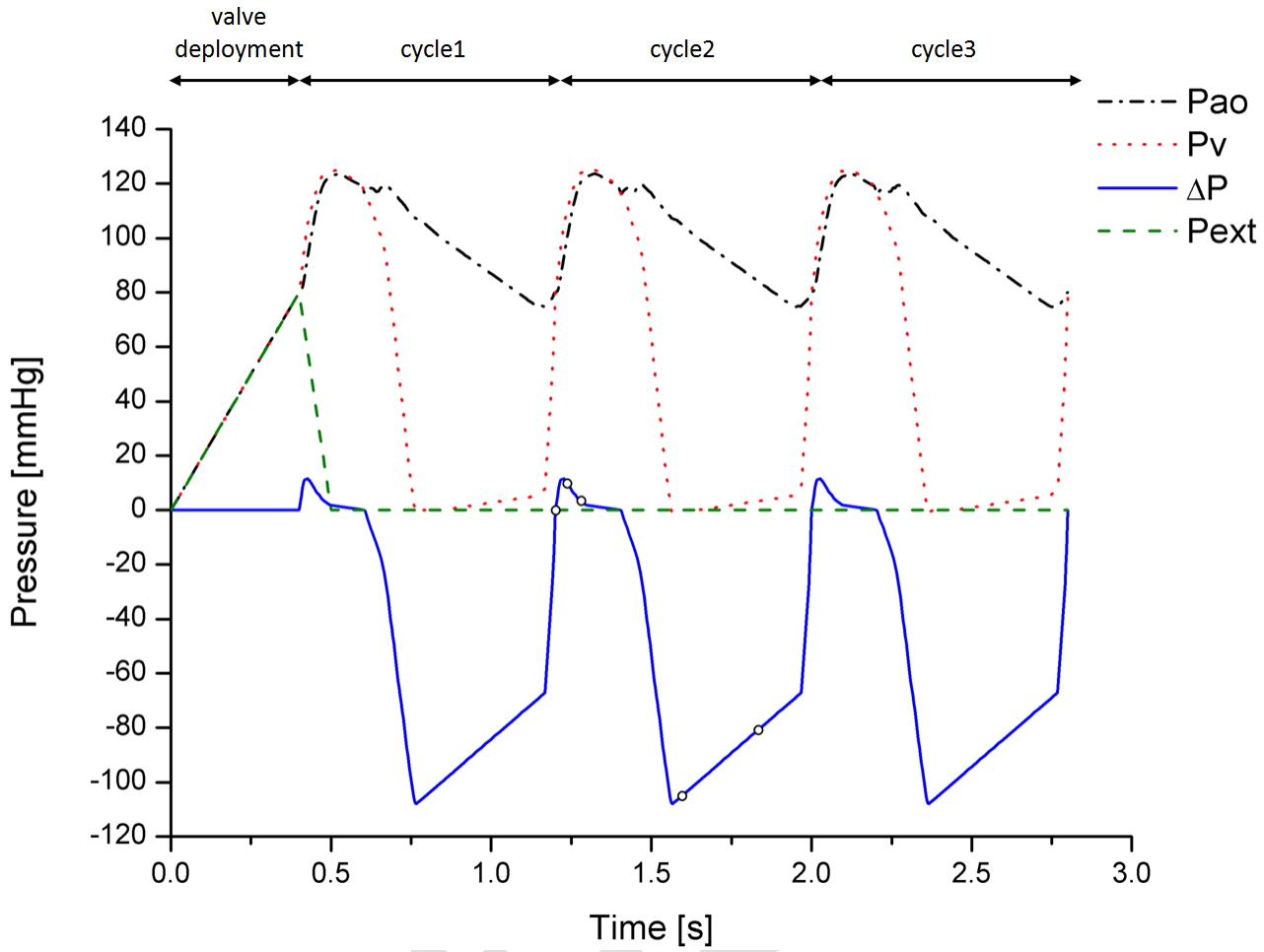


Figure 5. Aortic (ao), ventricular (v) and extramural (ext) pressure tracings applied in the patient-specific FSI simulation. The transvalvular gradient (ΔP) is also reported. At the beginning 0.4 s, there is a pressurization of 80 mmHg, and the valve was deployed in the AR. Circles on the ΔP are the time points to show the results.

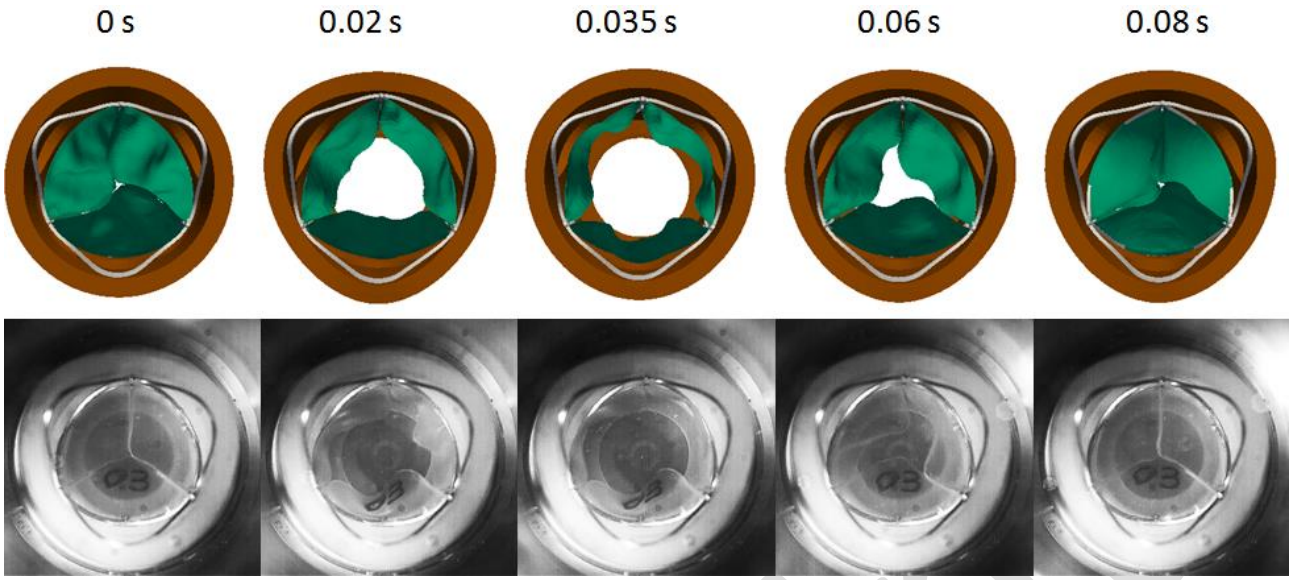


Fig. 6. Top views of the valve kinematics at five time instances for the FSI simulation (top) and the in vitro test (bottom). The leaflet thickness in the simulation was not displayed for a better visualization.

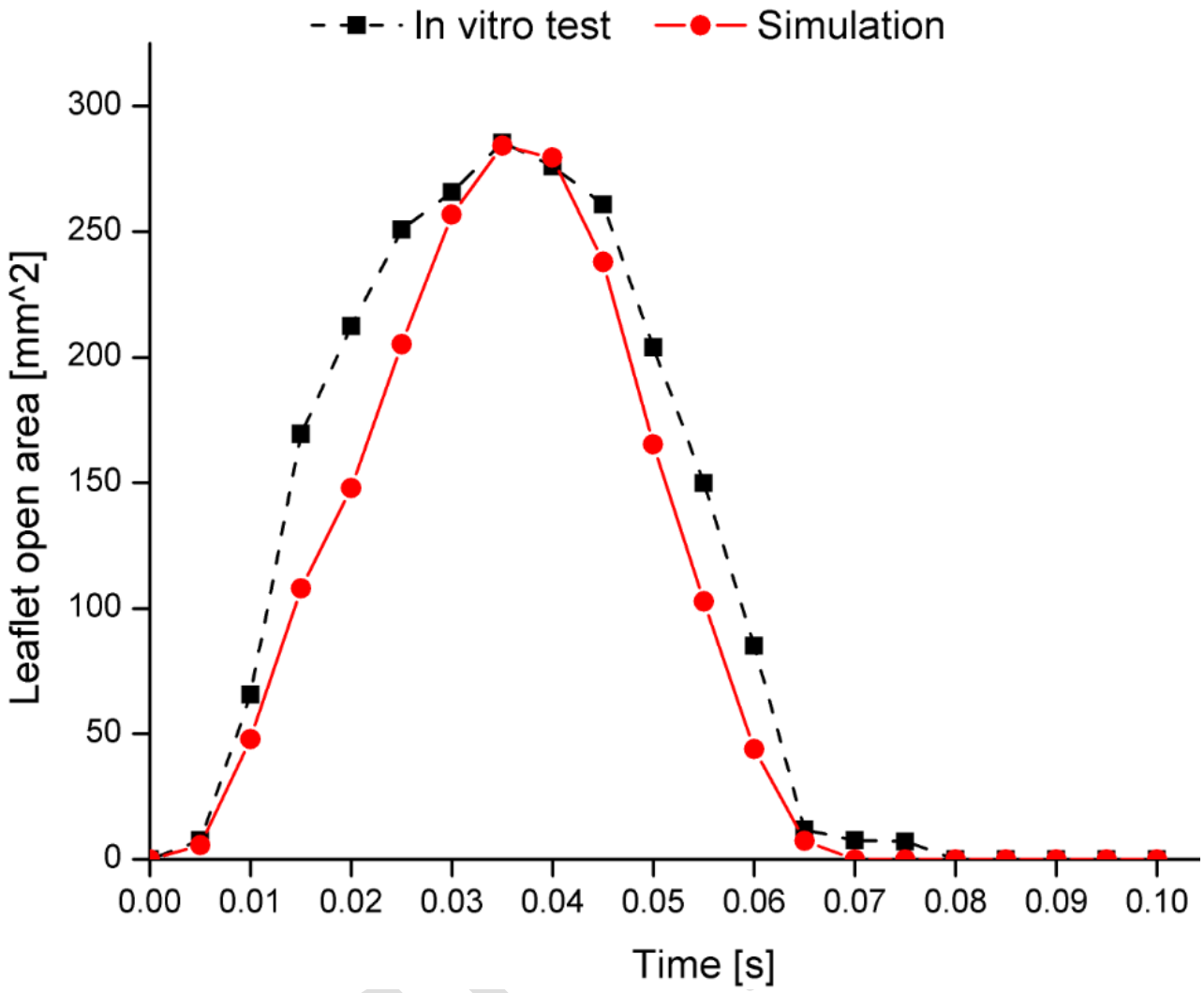


Fig. 7. Leaflet open areas of the in vitro test and in the FSI simulation during the period of 0.1 second.

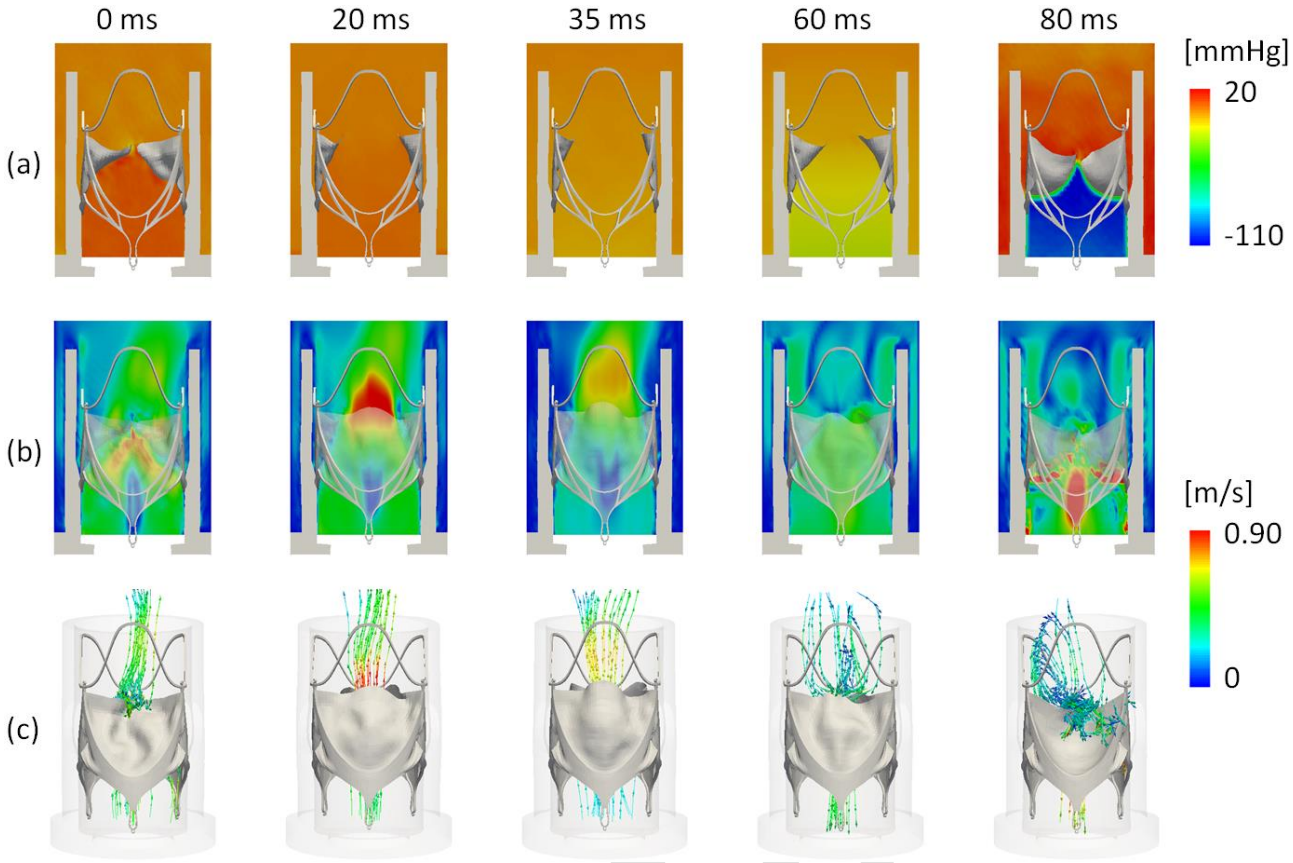


Fig. 8. Pressure (a) and velocity (b) contour maps of the in vitro FSI simulation. Pathlines colored with respect to velocities are also reported (c).

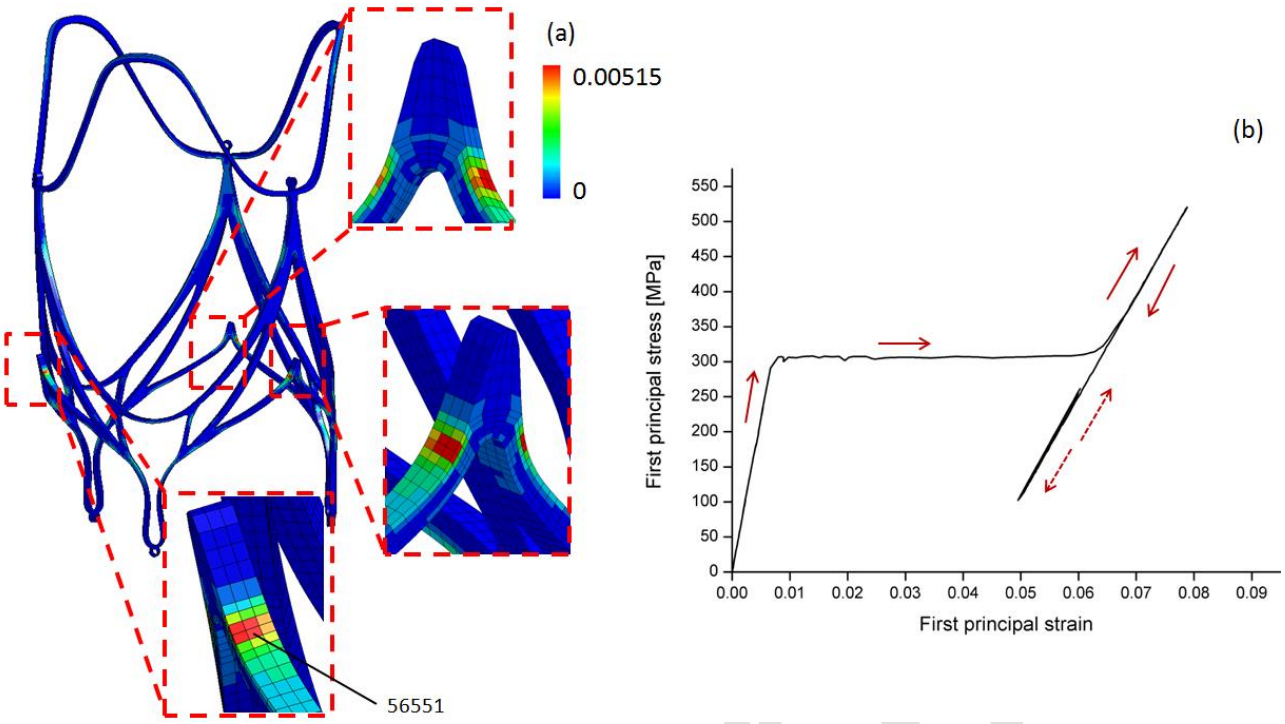


Figure 9. Alternating strain distribution in the stent frame of the in vitro simulation (a). The insets show the locations with the highest values. Element 56551 was chosen to show its stress-strain changes during the whole simulation (b). The solid arrows indicate the valve crimping and release, and the dashed arrows the fatigue cycles.

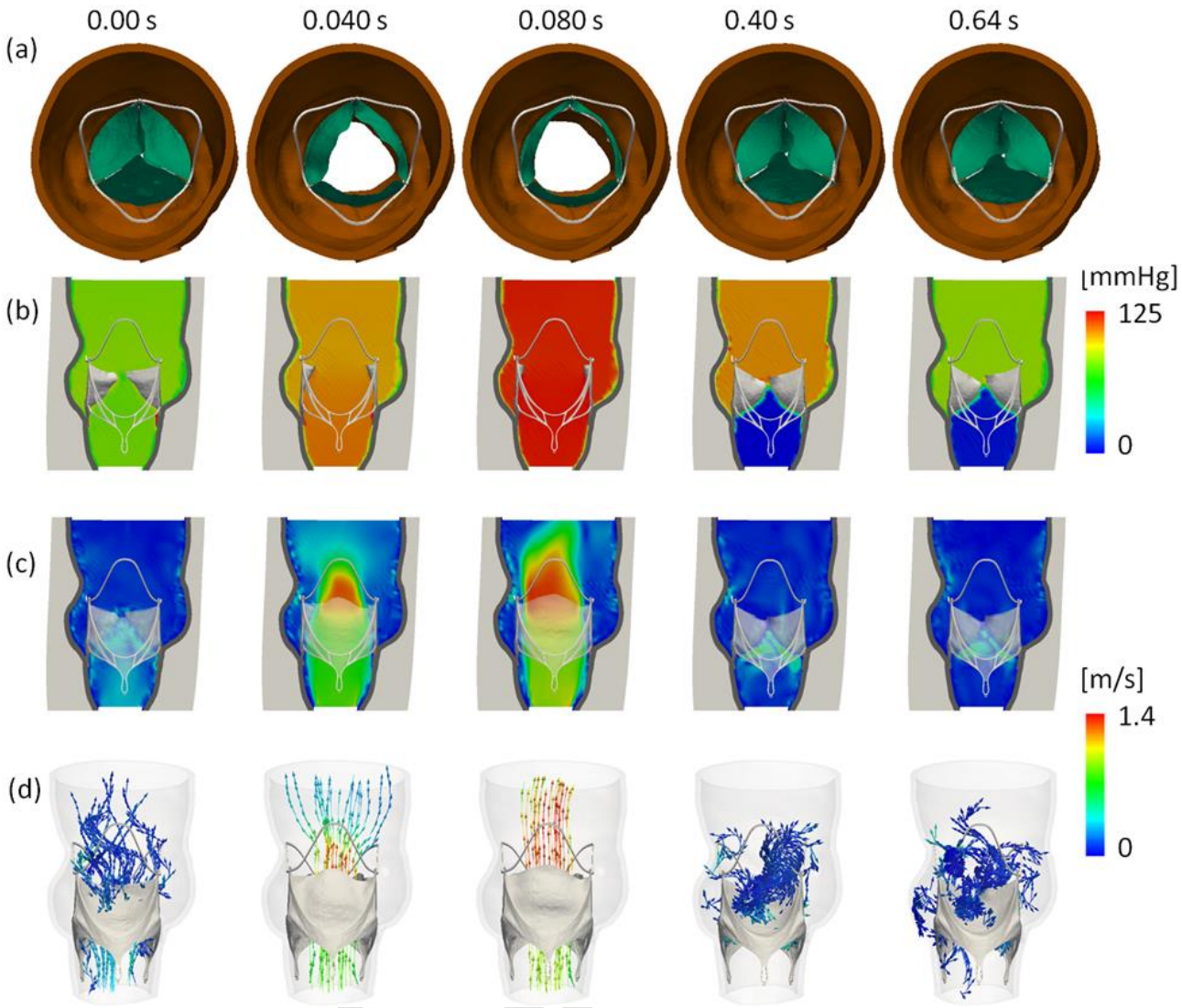


Figure 10. FSI patient-specific case: valve kinematics (a); pressure (b) and velocity (c) contour maps; pathlines coloured with respect to velocities (d).

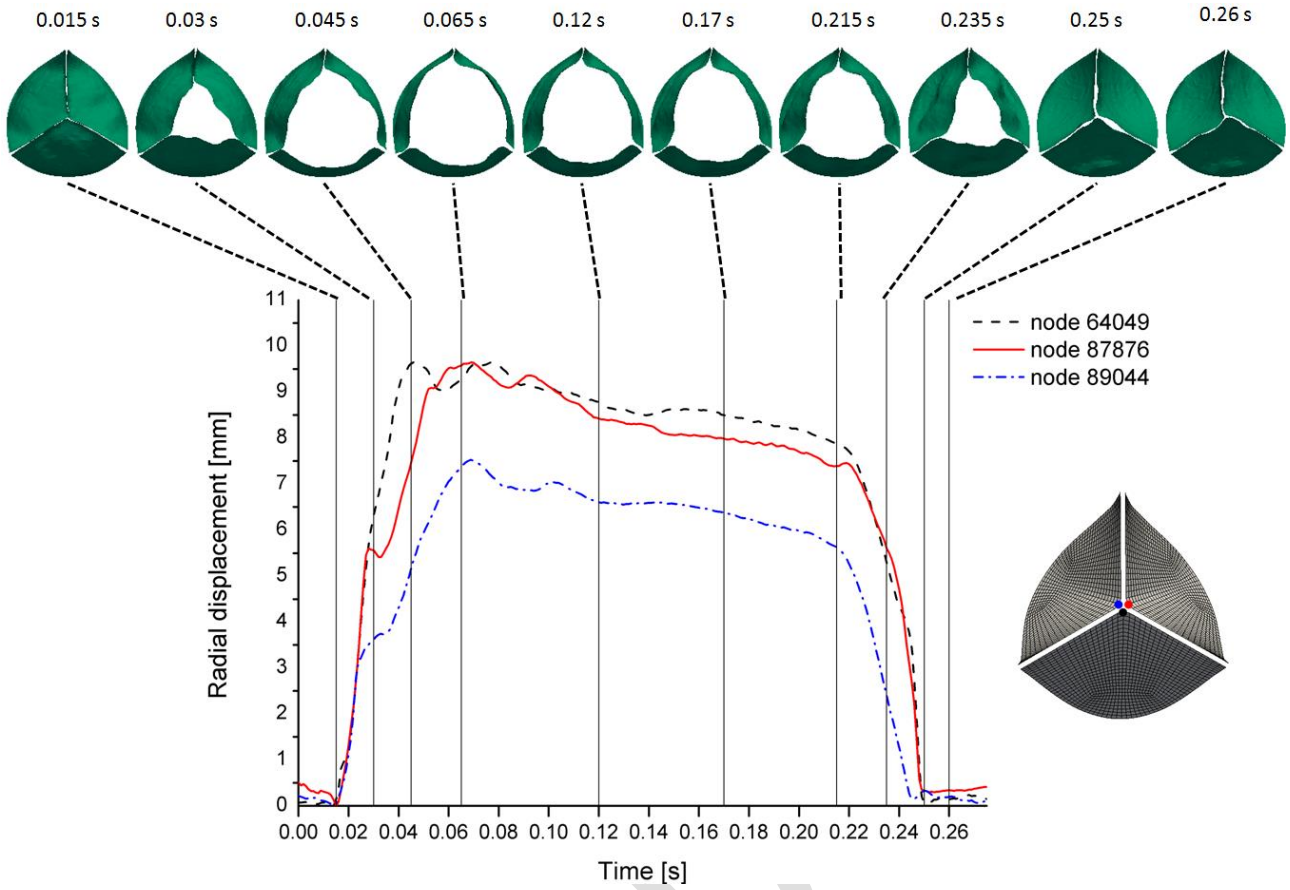


Figure 11. Detailed leaflet kinematics during systolic ejection (from 0 to 0.275 s of a cardiac cycle) indicating by both the radial displacement of the three upper-middle nodes of the leaflets and the deformation of the leaflets at different time points. The black, red and blue points on the leaflet mesh indicate the locations of node 64049, 87876 and 89044, respectively. The calculated rapid valve opening and closing times are shown in Table 3.

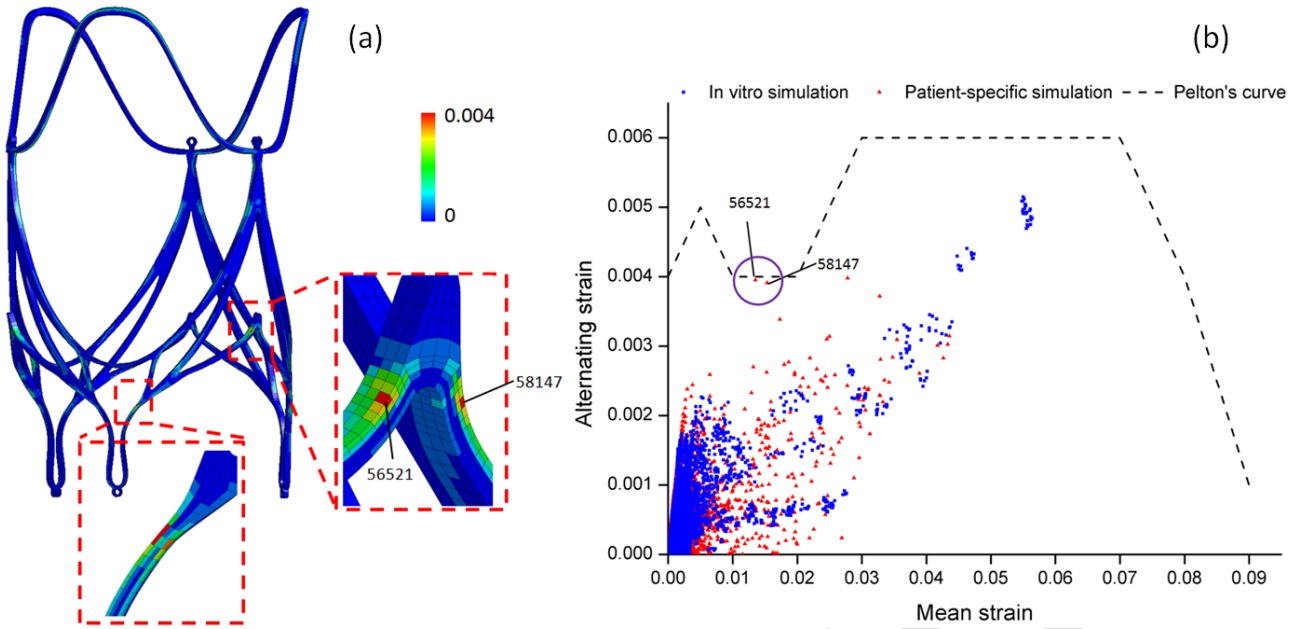


Figure 12. Alternating strain distribution in the stent frame of patient-specific simulation (left) and superimposed constant life diagrams of the valve for the in vitro and patient-specific cases (right). The circle indicate that there are two elements with alternating strain near the fatigue limit.

Accepted manuscript at https://doi.org/10.1007/s10439-015-1429-x

## Tables

Table 1. Contact definitions of the interacting model components

| Contact pairs | Normal interactions | Tangential interactions |
|---|---|---|
| Stent/leaflets | Node (leaflets) to surface (stent) tied algorithm | No sliding |
| Leaflet/leaflet | Surface to surface self-contact with penalty algorithm | Sliding with friction |
| Rigid planes/stent | Surface to surface contact with penalty algorithm | Sliding with friction |
| Stent/compartment ( or aortic root) | Surface to surface tied algorithm | No sliding |

Table 2. Mechanical properties of stent material

| $E_A$ [MPa] | $v$ | $\sigma_{AM}^S$ [MPa] | $\sigma_{AM}^F$ [MPa] | $\sigma_{MA}^S$ [MPa] | $\sigma_{MA}^F$ [MPa] | $\varepsilon_l$ | $\alpha$ | $E_M$ [MPa] |
|---|---|---|---|---|---|---|---|---|
| 45000 | 0.3 | 310 | 335 | 100 | 75 | 0.0426 | 0.19 | 15000 |

$E_A$and $E_M$, Young modulus of austenite (A) and martensite (M), respectively; $v$, Poisson's ration; $\sigma_{AM}^S$ and $\sigma_{AM}^F$, the starting and final stress value for the forward phase transformation (from A to M), respectively; $\sigma_{MA}^S$ and $\sigma_{MA}^F$, the starting and final stress value for the reverse phase transformation (from M to A), respectively; $\varepsilon_l$, the maximum transformation strain reached at the end of the A to M transformation; $\alpha$, the parameter measuring the difference between material responses in tension and compression.

Accepted manuscript at https://doi.org/10.1007/s10439-015-1429-x

Table 3. RVOT, RVCT and ET calculated by FSI simulation and measured in vivo

| | Node 89044 | Node 87876 | Node 64049 | Average of three nodes | In vivo data[21] |
|---|---|---|---|---|---|
| RVOT [ms] | 44 | 53 | 32 | 43 | 43.6±11.6 |
| RVCT [ms] | 32 | 31 | 31 | 31.3 | 31.5±8.8 |
| ET [ms] | 232 | 235 | 236 | 234 | 254±54 |

ET: ejection time; RVOT: rapid valve opening time; RVCT: rapid valve closing time.